Electronic Supplementary Information

Tuning the structure and catalytic activity of Ru nanoparticle catalysts by single 3d transition-metal atoms in Ru_{12}-metalloporphyrin precursors

Satoshi Muratsugu,*[a] Atsuki Yamaguchi,[a] Gen-ichi Yokota,[a] Tomoaki Maeno,[a] and Mizuki Tada*[a,b]

[a] Department of Chemistry, Graduate School of Science, Nagoya University, Furo-cho, Chikusa-ku, Nagoya, Aichi 464-8602, Japan.

[b] Research Center for Materials Science (RCMS) & Integrated Research Consortium on Chemical Science (IRCCS), Nagoya University, Furo-cho, Chikusa-ku, Nagoya, Aichi 464-8602, Japan.

Experimental Section

Materials and instruments

All chemicals were purchased from commercial sources (Wako Chemicals, Kishida Chemicals, Tokyo Chemical Industry, Sigma-Aldrich, Shin-Etsu Chemical, and Strem Chemicals) and used without further purification unless otherwise noted. Deuterated solvents were purchased from Cambridge Isotope Laboratories and used as received. SiO_2 (Aerosil 300, 300 m^2/g) was supplied by Nippon Aerosil Co. Ltd. The trinuclear ruthenium complex ($[Ru_3(\mu_3\text{-}O)(\mu\text{-}CH_3CO_2)_6(C_6H_5N)_2(CH_3OH)](PF_6)$) was synthesized according to a procedure in the literature.[1]

The ^1H and ^{13}C solution-state NMR spectra were measured at 293 K on an ECA600 spectrometer (JEOL) operating at 600 MHz. Me_4Si was used as the internal standard when chloroform-*d* was used as the solvent, and the residual solvent peaks were used as the internal standard for other deuterated solvents (1.96 ppm for acetonitrile-d_3 and 5.32 ppm for dichloromethane-d_2). ESI-TOF MS spectra were recorded on JMS-T100CS (JEOL) and LCT Premier XE (Waters) systems. MALDI-TOF MS spectra were recorded on AXIMA-CFR Plus (Shimadzu) and Ultraflex III (Bruker Daltonics) systems. 2-(4-Hydroxyphenylazo)benzoic acid (HABA) was used as a matrix, and insulin chain B oxidized was used as a control sample. UV/vis spectra were measured on a V-550 spectrometer (JASCO). The concentration of the sample solutions was 2.0×10^{-6} mol L^{-1} in dichloromethane.

Synthesis of copper 5,10,15,20-tetrakis(4-pyridyl)porphyrin[2,3]

Copper(II) acetate (0.31 g, 1.7×10^{-3} mol) was added to a suspension of 5,10,15,20-tetra(4-pyridyl)porphyrin (0.40 g, 6.5×10^{-4} mol) in a mixed solvent of *N*,*N*-dimethylformamide (DMF) (12 mL) and acetic acid (12 mL), and the mixture was refluxed for 48 h. The suspension was filtered, and the red-purple precipitate was washed with water and acetone and then extracted with 2,2,2-trifluoroethanol. The solvent was evaporated, the solid was triturated with acetone, and the red-purple solid was collected and dried under vacuum. Yield: 0.39 g (5.7×10^{-4} mol, 88%). ^1H NMR (600 MHz, chloroform-*d*/methanol-d_4 = 95/5 (v/v), ppm): δ 8.79 (s), 7.62 (s).

Synthesis of nickel 5,10,15,20-tetrakis(4-pyridyl)porphyrin[2,3,4]

Nickel(II) acetate tetrahydrate (0.21 g, 8.5×10^{-4} mol) was added to a suspension of 5,10,15,20-tetra(4-pyridyl)porphyrin (0.20 g, 3.3×10^{-4} mol) in a mixed solvent of DMF (12 mL) and acetic acid (12 mL), and the mixture was refluxed for 48 h. The suspension was filtered and the red-purple precipitate was washed with water and acetone and then dried under vacuum. Yield: 0.20 g (2.9×10^{-4} mol, 89%). ^1H NMR (600 MHz, chloroform-*d*/methanol-d_4 = 95/5 (v/v), ppm): δ 8.95 (d, 8H), 8.75 (s, 8H), 8.00 (d, 8H).

Synthesis of zinc 5,10,15,20-tetrakis(4-pyridyl)porphyrin[2,3,5]

Zinc(II) acetate (0.37 g, 2.0×10^{-3} mol) was added to a suspension of 5,10,15,20-tetra(4-pyridyl)porphyrin (0.20 g, 3.3×10^{-4} mol) in DMF (10 mL), and the mixture was refluxed for 48 h. The suspension was filtered, and the purple precipitate was washed with water and acetone and then dried under vacuum. Yield: 0.21 g (3.1×10^{-4} mol, 95%). ^1H NMR (600 MHz, chloroform-*d*/methanol-d_4 = 95/5 (v/v), ppm): δ 8.52 (s, 8H), 8.00–7.31 (s, 16H).

Synthesis of $Ru_{12}M$ complexes (1-$Ru_{12}M$, M = Cu, Ni, Zn) and monometallic Ru_{12} complex (1-Ru_{12})

Metal (copper, nickel, or zinc) 5,10,15,20-tetrakis(4-pyridyl)porphyrin/5,10,15,20-tetrakis(4-pyridyl)-21*H*,23*H*-porphine (4.0×10^{-5} mol) was added to a solution of $[Ru_3(\mu_3\text{-}O)(\mu\text{-}CH_3CO_2)_6(C_6H_5N)_2(CH_3OH)](PF_6)$ (0.16 g, 1.6×10^{-4} mol) in 2,2,2-trifluoroethanol (10 mL), and the resulting mixtures were stirred at room temperature for 19–20 h. Subsequently, the solutions were filtered and the collected dark green filtrates were reduced to about one-third of the original volume by rotary evaporation. The dark green powders were precipitated with diethyl ether (20–30 mL), filtered, and dried under vacuum. The obtained samples are denoted here as **1-$Ru_{12}M$** (M = Cu, Ni, Zn) and **1-Ru_{12}**.

1-Ru_{12}Cu: Yield: 0.126 g (2.7×10^{-5} mol, 69%). ^{1}H NMR (600 MHz, acetonitrile-d_3, ppm): δ = 6.43 (t), 6.00 (s), 5.65 (s), 4.82 (s), 4.60 (s), 0.69 (t), 0.14 (s). ESI-TOF MS (positive, methanol/dichloromethane = 1/1, Fig. I): *m*/*z*: 1002.09 $[M-4PF_6]^{4+}$ (calc. for $C_{128}H_{136}N_{16}O_{52}CuRu_{12}$: 1001.91).

1-Ru_{12}Ni: Yield: 0.143 g (3.1×10^{-5} mol, 80%). ^{1}H NMR (600 MHz, acetonitrile-d_3, ppm): δ = 7.46 (s, 8H), 6.41 (t, 8H), 6.01 (s, 8H), 5.60 (s, 16H), 4.88–4.69 (s, s, 36H), 0.66 (s, 8H), 0.00 (s, 16H). ESI-TOF MS (positive, methanol/dichloromethane = 1/1, Fig. I): *m*/*z*: 1001.09 $[M-4PF_6]^{4+}$ (calc. for $C_{128}H_{136}N_{16}O_{52}NiRu_{12}$: 1000.66).

1-Ru_{12}Zn[6]: Yield: 0.168 g (3.7×10^{-5} mol, 92%). ^{1}H NMR (600 MHz, acetonitrile-d_3, ppm): δ = 7.59 (s, 8H), 6.43 (t, 8H), 6.26 (s, 8H), 5.67 (s, 16H), 4.84–4.75 (s, s, 72H), 0.76 (s, 8H), 0.10 (s, 16H). ESI-TOF MS (positive, methanol/dichloromethane = 1/1, Fig. I): *m*/*z*: 1002.83 $[M\text{-}4PF_6]^{4+}$ (calc. for $C_{128}H_{136}N_{16}O_{52}ZnRu_{12}$: 1002.41).

1-Ru_{12}: Yield: 0.157 g (3.5×10^{-5} mol, 86%). ^{1}H NMR (600 MHz, acetonitrile-d_3, ppm): δ = 7.59 (s, 8H), 6.43 (t, 8H), 6.26 (s, 8H), 5.67 (s, 16H), 4.84–4.75 (s, s, 72H), 0.76 (s, 8H), 0.10 (s, 16H). ESI-TOF MS (positive, methanol/dichloromethane = 1/1): *m*/*z*: 986.14 $[M-4PF_6]^{4+}$ (calc. for $C_{128}H_{136}N_{16}O_{52}Ru_{12}$: 986.43).

Synthesis of copper 5,10,15,20-tetraphenylporphyrin[7]

Copper(II) acetate monohydrate (0.0793 g, 4.0×10^{-4} mol) was added to a solution of 5,10,15,20-tetraphenylporphyrin (0.243 g, 4.0×10^{-4} mol) in a mixed solvent of methanol (12 mL) and toluene (40 mL), and the mixture was refluxed for 4 h. The suspension was filtered, and the red-purple precipitate was washed with methanol and toluene and then dried under vacuum. Yield: 0.151 g (2.2×10^{-4} mol, 56%). ^{1}H NMR (600 MHz, chloroform-*d*, ppm): δ 7.65 (br), 7.49 (br). MALDI-TOF MS (positive, HABA): *m*/*z*: 675.80 $[M]^+$ (calc. for $C_{44}H_{28}CuN_4$: 676.28).

Preparation of 4-pyridylethyltriethoxysilane-functionalized SiO_2 (A)[8]

SiO_2 (Aerosil 300, 6.0 g, 300 m^2/g) was calcined at 673 K for 2 h and then maintained under vacuum while cooling. The precalcined SiO_2 was suspended in dry toluene (120 mL) under an N_2 atmosphere, and a dry toluene solution (10 mL) of 4-pyridylethyltriethoxysilane (Py-et-Si(OEt)$_3$; 0.30 mL, 1.1×10^{-3} mol, to give a surface density of 0.30 nm^{-2} of Py groups on the SiO_2 surface when assuming 100% grafting) was added. This suspension was refluxed for 24 h. After cooling to room temperature, the resulting gel was collected in a thimble filter tube inside a Schlenk flask and washed with toluene, followed by washing with toluene in a Soxhlet extractor for about 22 h and then with hexane for about 16 h under N_2. Finally, the gel was dried under vacuum. The obtained sample is denoted here as **A**. The actual average surface density of Py groups was estimated to be 0.27 nm^{-2} from the N content determined by elemental analysis (N: 0.18%).

Preparation of B-Ru_{12}M, B-Ru_{12}, and B-Cu: Attachment of 1-Ru_{12}M to A

Under an N_2 atmosphere, solutions of **1-Ru_{12}M** (M = Cu, Ni, Zn) (0.090 g, 2.0×10^{-5} mol), **1-Ru_{12}** (0.090 g, 2.0×10^{-5} mol), or **1-Cu** (0.013 g, 2.0×10^{-5} mol) in dry degassed dichloromethane (10 mL) were added to suspensions of **A** (2 g, average surface density of pyridine moiety: 0.27 nm^{-2}) in dry degassed dichloromethane (18 mL). The suspensions were stirred at 298 K for 1 h. Subsequently, the mixtures were dried under vacuum to afford green solids, which are denoted here as **B-Ru_{12}M**, **B-Ru_{12}**, and **B-Cu** respectively. The loading of each metal was estimated by X-ray fluorescence (XRF) spectroscopy.

The surface density of **1-Ru_{12}M** on **B** was estimated using the following equation.

The surface density of **1-Ru_{12}M** = The number of **1-Ru_{12}M** (6×10^{18}/ 1 g of SiO_2)

/ The surface area of SiO_2 (300 m^2/g)

Preparation of C-Ru_{12}M, C-Ru_{12}, and C-Cu[9]

Tetramethoxysilane (Si(OCH$_3$)$_4$, TMOS) (2.5 mL) and distilled H_2O (1.2 g) were placed in two glass reactors (made by glass tubes) connected to a two-necked flask containing **B-Ru_{12}M**, **B-Ru_{12}**, or **B-Cu** (1.5 g). Ribbon heaters and thermal insulators were wrapped on the two glass reactors and the connected glass tube. After the whole system was evacuated to prepare a closed system with reduced pressure (ca. 1 Pa) for 0.5 h, the glass reactors were heated to 383 K and chemical vapor deposition (CVD) was utilized to vaporize TMOS and H_2O and deposit them on **B-Ru_{12}M**, **B-Ru_{12}**, or **B-Cu**. During the CVD process, **B-Ru_{12}M**, **B-Ru_{12}**, or **B-Cu** in the two-necked flask was vigorously stirred at room temperature. Then, the two-necked flask was separated while maintaining the closed system, and hydrolysis–polymerization of TMOS was performed at 353 K for 24 h in an oven. The whole closed system was subsequently evacuated at 373 K for 3 h. The obtained samples are denoted here as **C-Ru_{12}M**, **C-Ru_{12}**, and **C-Cu**. The loading of each metal was estimated by XRF.

The amount of SiO_2 matrix overlayers was estimated to be the weight gain after the preparation process of **C**-series, and the average weight gain was 1.0 g. The structure of SiO_2 matrix overlayers was assumed to be quartz (density = 2.2 g cm^{-3}) to calculate the average height of SiO_2 matrix overlayres, although the actual structure of SiO_2 matrix overlayers is amorphous. From these data, the average height of SiO_2 matrix overlayres was estimated to be 1 nm.[9]

Preparation of D-RuM, D-Ru, and D-Cu

C-Ru$_{12}$M, **C-Ru$_{12}$**, or **C-Cu** was placed in a glass flow cell, which was then attached to a vacuum line. After evacuating the cell (ca. 10^{-2} Pa), it was heated to 873 K and held at that temperature for 2 h. Subsequently, H_2 (6.7 kPa) was passed through the cell for 1 h at 873 K. The obtained black solids are denoted here as **D-RuM**, **D-Ru**, and **D-Cu**. The loading of each metal was estimated by XRF.

Catalyst characterization

XRF: XRF was measured on a JSX-1000S spectrometer (JEOL) operating at room temperature. The loadings of Ru, Cu, Ni, and Zn were estimated from the Ru/Si, Cu/Si, Ni/Si, and Zn/Si peak intensity ratios, respectively, using standard curves based on the Ru K_α, Cu K_α, Ni K_α, Zn K_α, and Si K_α fluorescence X-rays (the net counts were used). The samples were thoroughly ground using a mortar and pestle, and 20 mg samples were pressed (1 MPa) into pellet disks for the measurements. The samples used for generating the standard curves for Ru/Si, Cu/Si, Ni,/Si, and Zn/Si were prepared by the impregnation of SiO_2 (Aerosil 300) with di-μ-chlorobis[(*p*-cymene)chlororuthenium], bis(2,4-pentanedionato)copper, [1,2-bis(diphenylphosphino)ethane]dichloronickel, and bis(2,4-pentanedionato)zinc using dichloromethane.

UV/vis spectroscopy: Diffuse reflectance (DR) UV/vis spectra of solid samples were measured on a V-550 spectrometer (JASCO). Each solid sample was enclosed in a quartz cell under Ar and the DR-UV/vis spectra were recorded using an integrating sphere.

Elemental analysis: Organic residues on the solid samples were analyzed by elemental analysis (Microorganic Element Analyzer CHN Corder MT-6, Yanako). The surface loadings of the pyridine ligand and metal complexes were estimated from the value of N wt %.

Powder X-ray diffraction (XRD): Powder XRD patterns with a wide angle range (3–90°) were recorded at a scan rate of 2° min^{-1} using a MultiFlex X-ray diffractometer (Rigaku; Cu K_α, λ = 1.5418 Å, 40 kV, 30 mA), and those with a narrow angle range (30–48°) were measured at a scan rate of 3.4° min^{-1} using an Empyrean X-ray diffractometer (PANalytical; Cu K_α, λ = 1.5418 Å, 45 kV, 40 mA).

X-ray photoelectron spectroscopy (XPS): XPS was measured on an ECSA3057 system (ULVAC-PHI) at a base pressure of 1×10^{-7} Pa. The X-ray source and power were Al Kα (1486.7 eV) and 350 W, respectively. Narrow multiplex scans were recorded with a pass energy of 11.75 eV and a step size of 0.1 eV. A charge neutralization function was employed to compensate for the charge buildup on the solid samples due to X-ray irradiation. The samples were ground and pressed into pellet disks (10 mg pressed at 2–5 MPa), which were attached to the cell holder using carbon tape. Background subtraction was performed according to the Shirley method using the Origin software (version 8), and each peak was curve fitted using Gaussian waves. The binding energies were referenced to Si 2p at 103.4 eV and the peak intensities were normalized using the peak areas from the Si 2p XPS spectra.

X-ray absorption fine structure (XAFS): XAFS spectra at the Ru K-edge were measured in the transmission mode at the NW10A station of the Photon Factory at KEK-IMSS (Tsukuba, Japan). The energy and current of the electrons in the storage ring were 6.5 GeV and 60 mA, respectively. X-rays from the storage ring were monochromatized using a Si(311) double-crystal monochromator, and ionization chambers filled with pure Ar and Kr gases were used to monitor the incident and transmitted X-rays, respectively. Ru powder mixed with boron nitride and pelletized into a disk (10 mm in diameter) was used as the reference. All of the samples were enclosed in an XAFS cell (4 mmϕ) sealed with a carbon cap inside a glovebox without exposure to air. All of the samples were measured at 20 K under vacuum.

XAFS spectra at the Cu, Ni, and Zn K-edges were measured in the fluorescence mode at the BL12C station of the Photon Factory at KEK-IMSS (Tsukuba, Japan). The energy and current of the electrons in the storage ring were 6.5 GeV and 60 mA, respectively. X-rays from the storage ring were monochromatized with a

Si(111) double-crystal monochromator. Two ionization chambers filled with pure N_2 gas and a mixture of N_2 and Ar gases (1/1, v/v), and a 19-channel germanium multi-solid-state detector (MSSD) were used to monitor the incident, transmitted, and fluorescence X-rays, respectively. For Ni K-edge, the intensity of incident X-ray was detune to 70% of initial intensity. Inelastically scattered X-rays from Cu, Ni, and Zn were cut off with Ni, Co, and Cu filters (μt = 6), respectively, and the fluorescence X-rays from each element (K_α line) were selected. All of the samples were enclosed in an XAFS cell (4 mmϕ, 2 mm thickness) sealed with Kapton tape inside a glovebox without exposure to air. All of the samples were measured at 20 K under vacuum.

The XAFS spectra were analyzed using ATHENA and ARTEMIS with IFEFFIT (version 1.2.11).[10] The threshold energy was tentatively set at the inflection point of the Ru K-edge (22118.0 eV), Cu K-edge (8980.0 eV), Ni K-edge (8331.0 eV), or Zn K-edge (9660.7 eV).[11] Background subtraction was performed using the Autobk method and the spline smoothing algorithm in ATHENA.[12] The k^3-weighted extended XAFS (EXAFS) oscillations were Fourier transformed into *R*-space. Curve-fitting analysis was carried out in the *R*-space. The fitting parameters for each shell were the coordination number (CN), interatomic distance (*R*), Debye–Waller factor (σ^2: mean-square displacement), and correction-of-edge energy (ΔE_0). The ΔE_0 and σ^2 of Ru–O (μ-O), Ru–O (CH_3COO), Ru–N (py), Ru···C (CH_3COO, py), and Ru–O in **D**-series were restrained to be the same values in the Ru K-edge EXAFS curve-fitting analyses. The values of S_0^2 were estimated using the EXAFS curve fitting of standard samples, and were fixed for each EXAFS analysis. For the Ru K-edge, S_0^2 was fixed to be 1 (from Ru powder and **1-Ru_{12}Cu**). For the Cu K-edge, S_0^2 was fixed to be 0.97 (from **1-Ru_{12}Cu**) for the curve fitting of **B-Ru_{12}Cu** and **C-Ru_{12}Cu** or CuO (0.67) for **D-RuCu**. For the Ni K-edge, S_0^2 was fixed to be 0.73 (from **1-Ru_{12}Ni**) for the curve fitting of **B-Ru_{12}Ni** and **C-Ru_{12}Ni** or NiO (0.92) for **D-RuNi**. For the Zn K-edge, S_0^2 was fixed to be 0.82 (from **1-Ru_{12}Zn**) for the curve-fitting of **B-Ru_{12}Zn** and **C-Ru_{12}Zn** or ZnO (0.92) for **D-RuZn**. The phase shifts and backscattering amplitudes were calculated using the FEFF8[13] code with the structural parameters obtained from the crystal structures of Ru metal, CuO, NiO, ZnO, $[Ru_3(\mu_3\text{-}O)(\mu\text{-}CH_3CO_2)_6(C_6H_5N)_3](PF_6)$,[14] 5,10,15,20-tetraphenylporphyrin Cu complex,[15] 2,3,7,8,12,13,17,18-octaethylporphinato Ni complex,[16] and 5,15-bis(3,5-di-*t*-butylphenyl)-10,20-diphenylporphinato Zn complex.[17]

High-angle Annular Dark Field Scanning Transmission Electron Microscopy (HAADF-STEM): HAADF-STEM images were taken using a JEM-ARM 200F transmission electron microscopes (JEOL with an accelerating voltage of 200 kV High Voltage Electron Microscope Laboratory, Institute of Materials and Systems for Sustainability, Nagoya University, Japan). Samples were directly deposited on an appropriate microgrid (Cu, Mo, Ni) and were blown with an air duster gun to remove excess. Carbon deposition was conducted on the microgrids using a carbon coater in order to minimize the drift of the samples during measurement.

Catalytic reactions

Hydrogenation of acetophenone derivatives: The appropriate catalyst (Ru: 1.1×10^{-6} mol) was transferred into a glass tube inside an Ar-filled glove box, and a solution of acetophenone (5.3×10^{-4} mol, 0.18 mol L^{-1}) in dry, degassed 1,4-dioxane (3 mL) was added. The glass tube was placed in an autoclave under an N_2 atmosphere. The system was then purged with H_2 (0.5 MPa) and leaked to atmospheric pressure. This cycle was repeated ten times to exchange the inner atmosphere of the autoclave to H_2. The system was then purged with 2.0 MPa of H_2, and the reaction mixture was stirred at 363 K. After the reaction, the H_2 was leaked and the solid portion of the reaction mixture was removed by filtration. *n*-Dodecane (0.010 mL, 4.4×10^{-5} mol) was added to a sample (0.5 mL) of the solution portion as an internal standard. The molar ratio of Ru to the reactant and the internal standard was maintained at 1:500:250. The reactions were monitored using FID-GC (Shimadzu GC-2014) and GC-MS (Shimadzu GC-MS QP2010) with an InertCap 5 column (GL Science, 0.25 μm (df) × 0.25 mm (I.D.) × 30 m).

Heterogeneity test: The reaction conducted using the above procedure, and the solution phase was separated from the solid part at the point where the conversion of acetophenone was around 20% under N_2 atmosphere. The solution phase was continued for the reaction and the GC analysis was performed in a similar way.

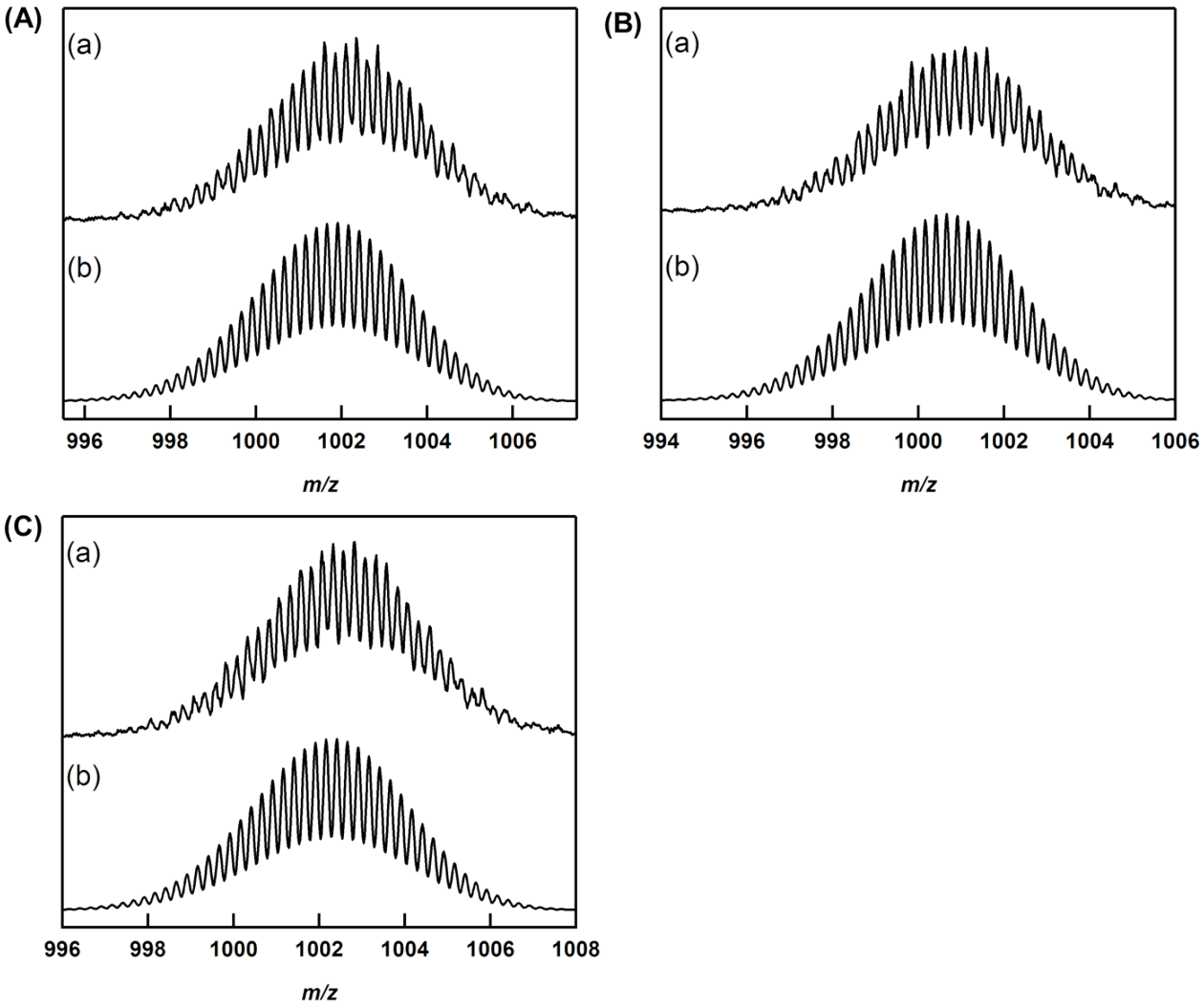

Fig. I. ESI-TOF MS spectra of (A) **1-Ru_{12}Cu**, (a) an observed spectrum and (b) a simulated spectrum for $[C_{128}H_{136}N_{16}O_{52}CuRu_{12}]^{4+}$; (B) **1-$Ru_{12}$Ni**, (a) an observed spectrum and (b) a simulated spectrum for $[C_{128}H_{136}N_{16}O_{52}NiRu_{12}]^{4+}$; and (C) **1-$Ru_{12}$Zn**, (a) an observed spectrum and (b) a simulated spectrum for $[C_{128}H_{136}N_{16}O_{52}ZnRu_{12}]^{4+}$.

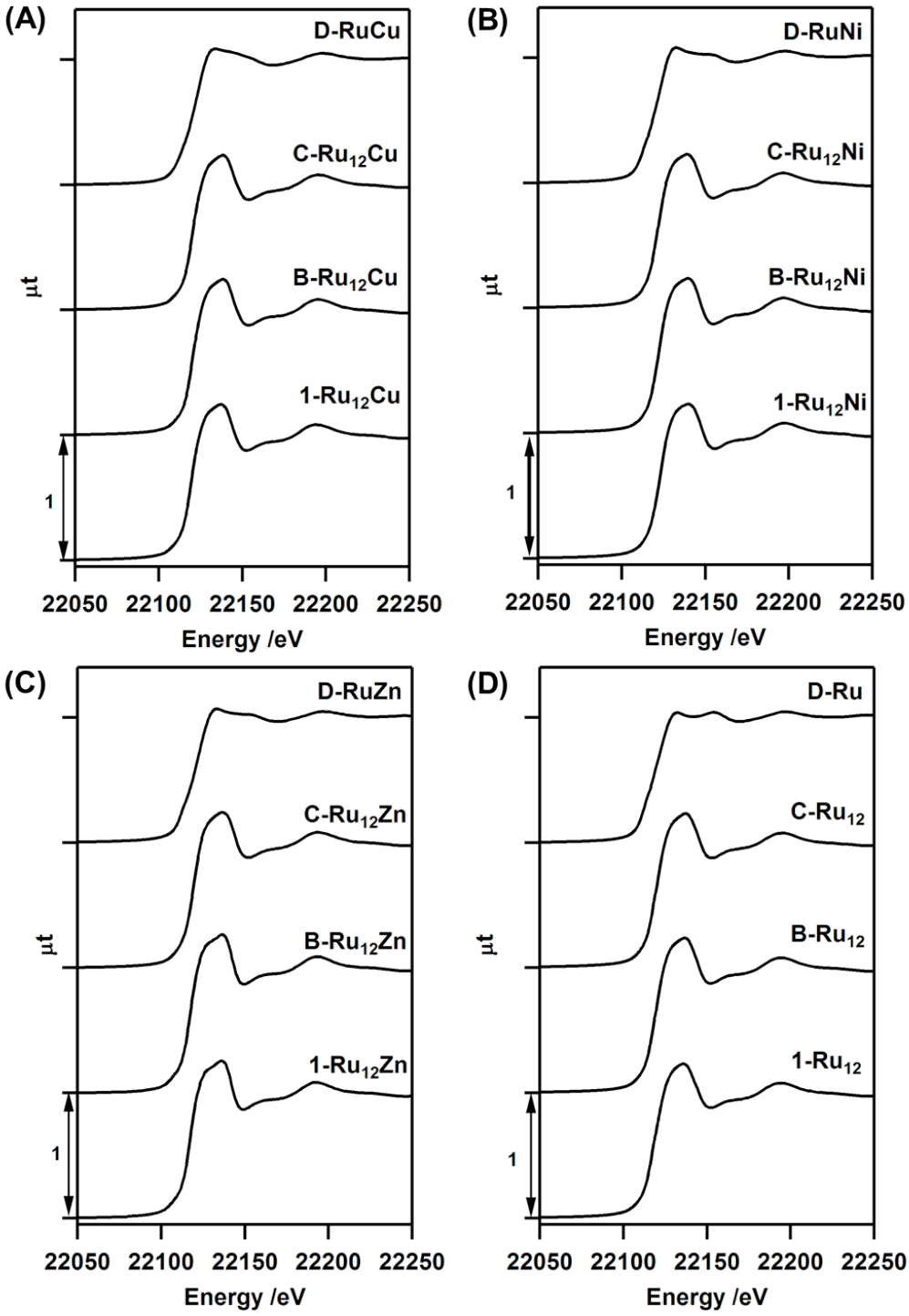

Fig. S1. Normalized Ru K-edge XANES spectra of (A) **1-Ru$_{12}$Cu**, **B-Ru$_{12}$Cu**, **C-Ru$_{12}$Cu**, and **D-RuCu**; (B) **1-Ru$_{12}$Ni**, **B-Ru$_{12}$Ni**, **C-Ru$_{12}$Ni**, and **D-RuNi**; (C) **1-Ru$_{12}$Zn**, **B-Ru$_{12}$Zn**, **C-Ru$_{12}$Zn**, and **D-RuZn**; and (D) **1-Ru$_{12}$**, **B-Ru$_{12}$**, **C-Ru$_{12}$**, and **D-Ru**. All of the samples were measured at 20 K.

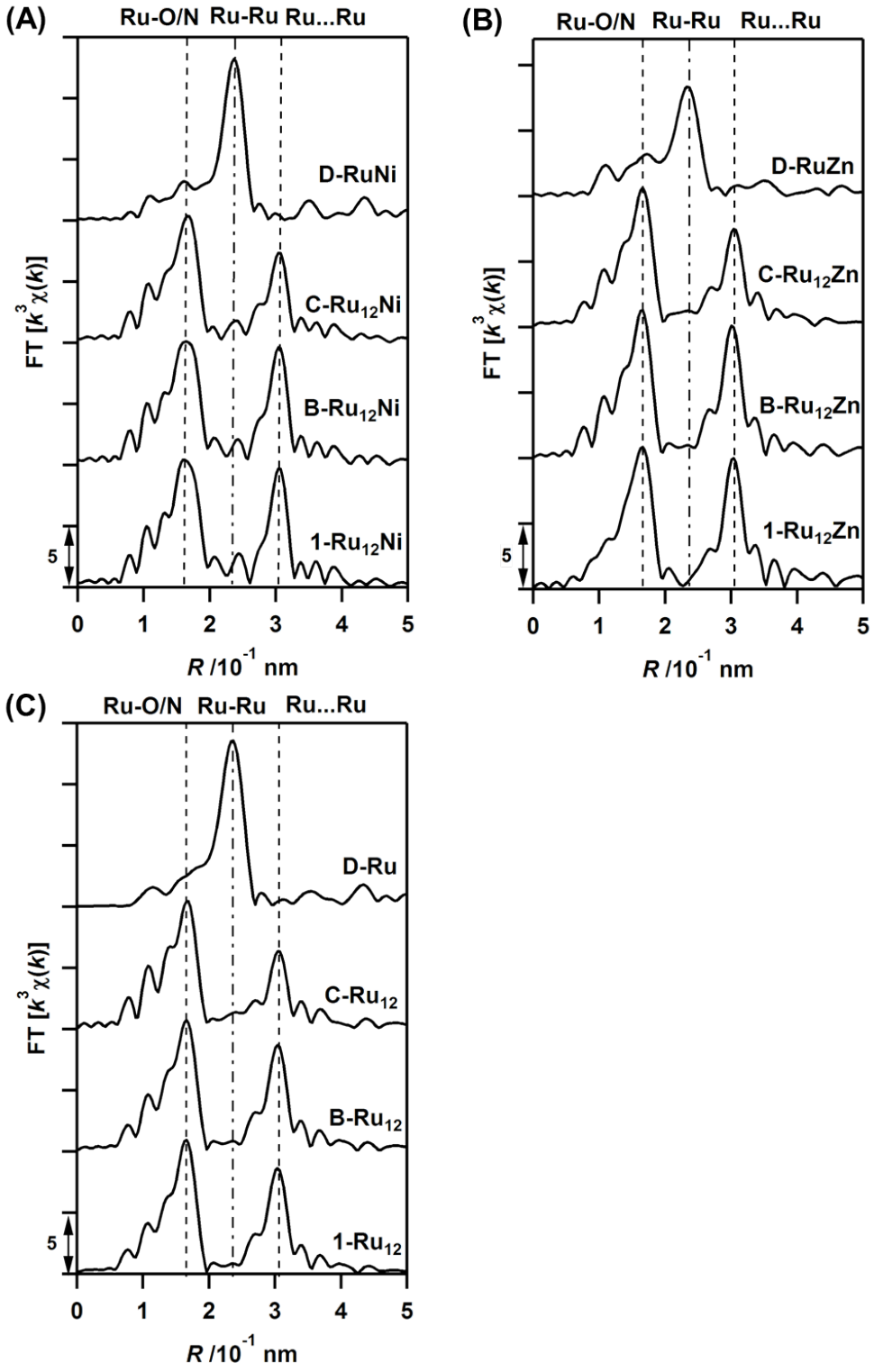

Fig. S2. k^3-Weighted Ru K-edge EXAFS Fourier transforms (k = 30–160 nm^{-1}) for (A) **1-Ru$_{12}$Ni**, **B-Ru$_{12}$Ni**, **C-Ru$_{12}$Ni**, and **D-RuNi**; (B) **1-Ru$_{12}$Zn**, **B-Ru$_{12}$Zn**, **C-Ru$_{12}$Zn**, and **D-RuZn**; and **1-Ru$_{12}$**, **B-Ru$_{12}$**, **C-Ru$_{12}$**, and **D-Ru**. All of the samples were measured at 20 K.

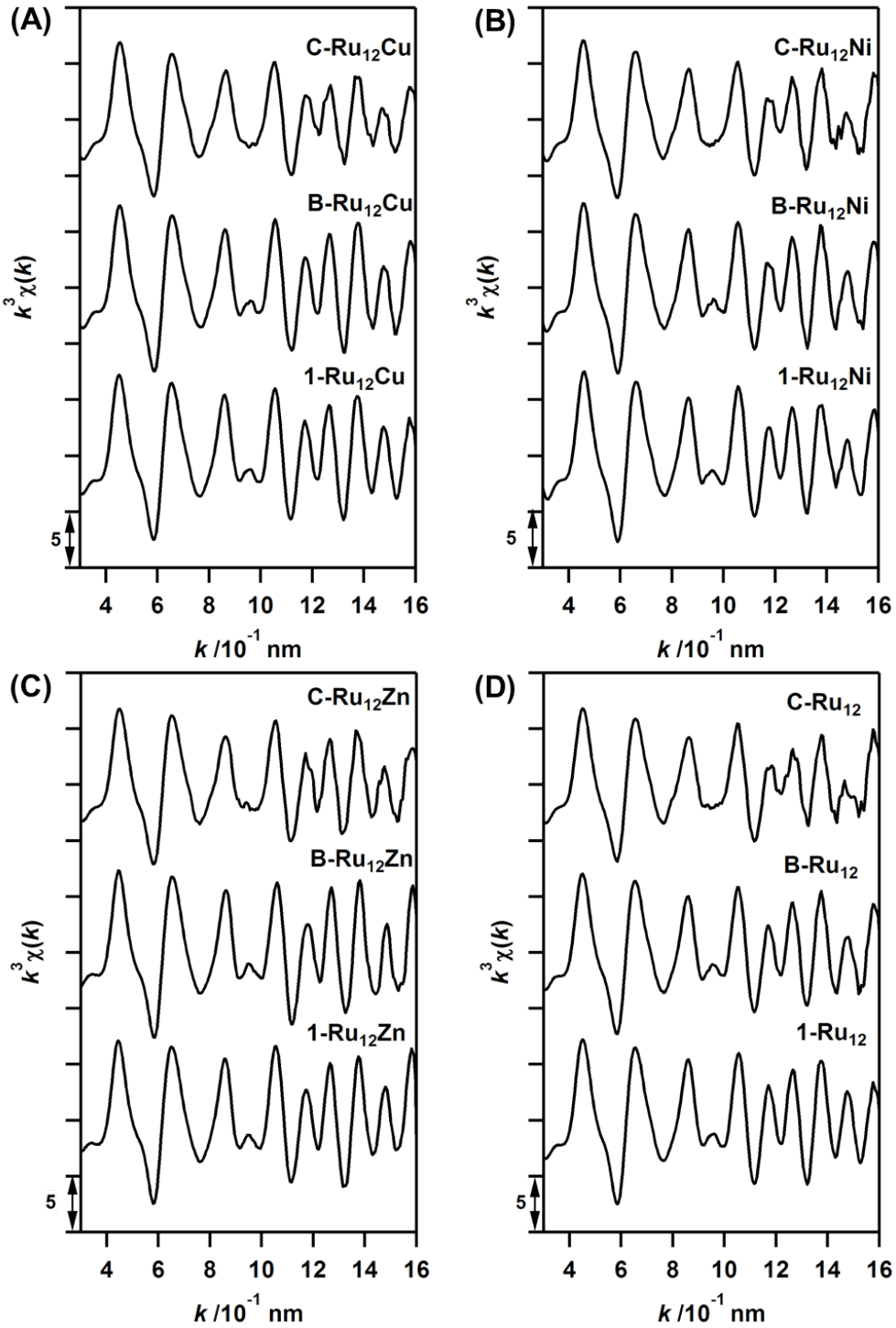

Fig. S3. k^3-Weighted Ru K-edge EXAFS oscillations of (A) **1-Ru$_{12}$Cu**, **B-Ru$_{12}$Cu**, and **C-Ru$_{12}$Cu**; (B) **1-Ru$_{12}$Ni**, **B-Ru$_{12}$Ni**, and **C-Ru$_{12}$Ni**; (C) **1-Ru$_{12}$Zn**, **B-Ru$_{12}$Zn**, and **C-Ru$_{12}$Zn**; and (D) **1-Ru$_{12}$**, **B-Ru$_{12}$**, and **C-Ru$_{12}$**. All of the samples were measured at 20 K.

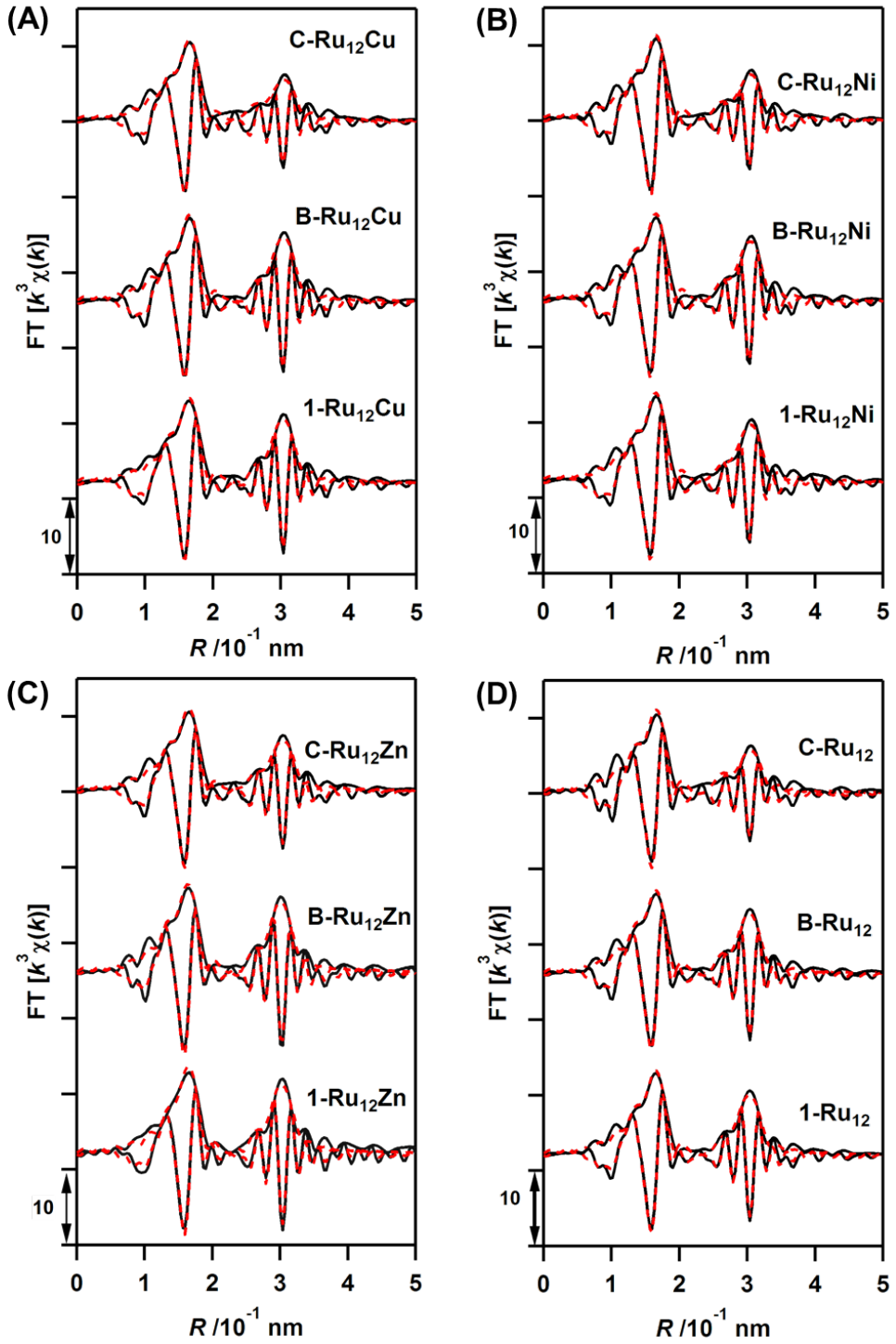

Fig. S4. k^3-Weighted Ru K-edge EXAFS Fourier transforms (k = 30–160 nm^{-1}) for (A) **1-Ru$_{12}$Cu**, **B-Ru$_{12}$Cu**, and **C-Ru$_{12}$Cu**; (B) **1-Ru$_{12}$Ni**, **B-Ru$_{12}$Ni**, and **C-Ru$_{12}$Ni**; (C) **1-Ru$_{12}$Zn**, **B-Ru$_{12}$Zn**, and **C-Ru$_{12}$Zn**; and (D) **1-Ru$_{12}$**, **B-Ru$_{12}$**, and **C-Ru$_{12}$**. All of the samples were measured at 20 K. The black solid lines show the observed data and the red dashed lines show the fitted data.

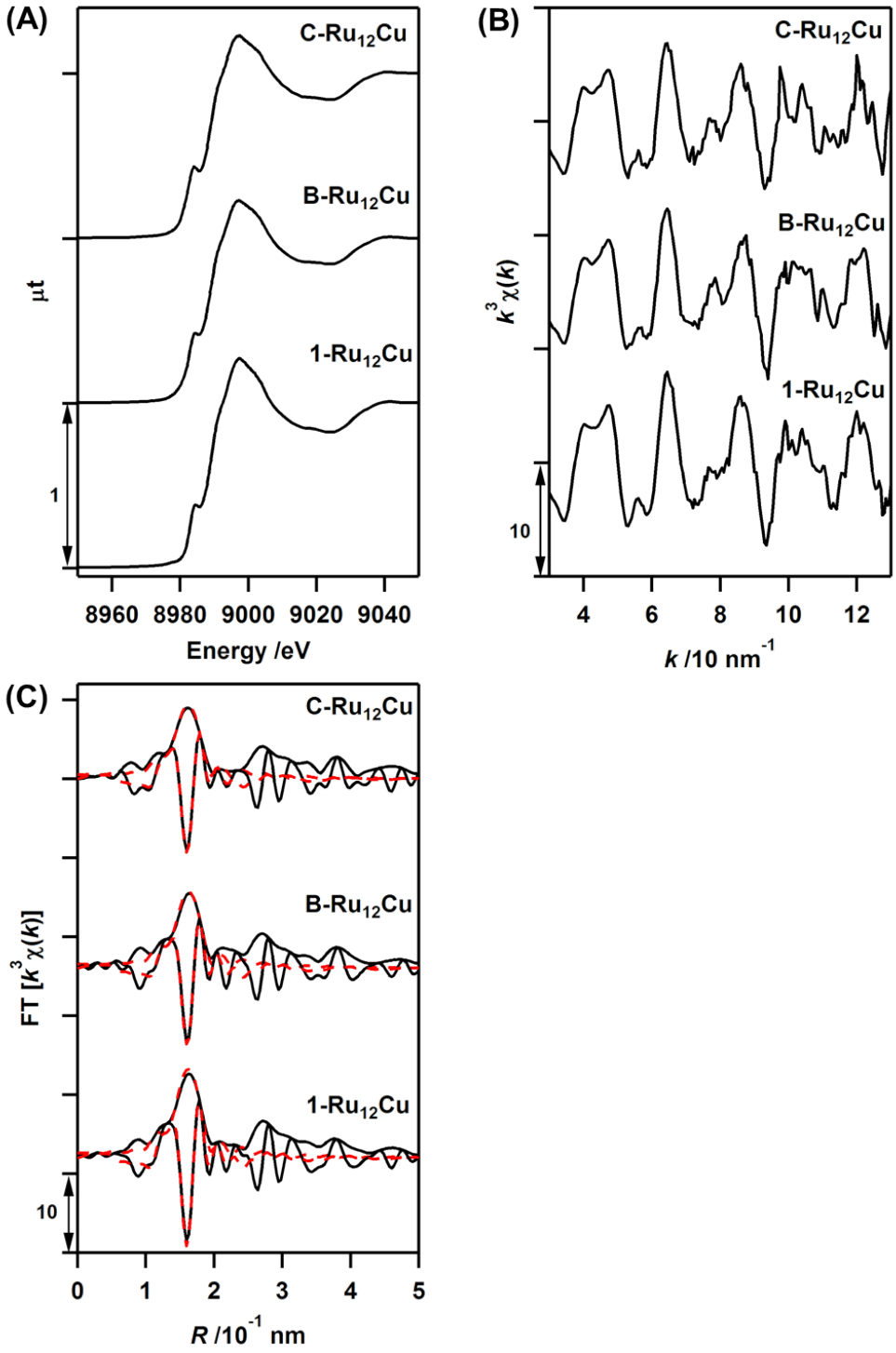

Fig. S5. (A) Normalized Cu K-edge XANES spectra, (B) k^3-weighted Cu K-edge EXAFS oscillations, and (C) their Fourier transforms (k = 30–130 nm^{-1}) for **1-Ru$_{12}$Cu**, **B-Ru$_{12}$Cu**, and **C-Ru$_{12}$Cu**. All of the samples were measured at 20 K. In (C), the black solid lines show the observed data and the red dashed lines show the fitted data.

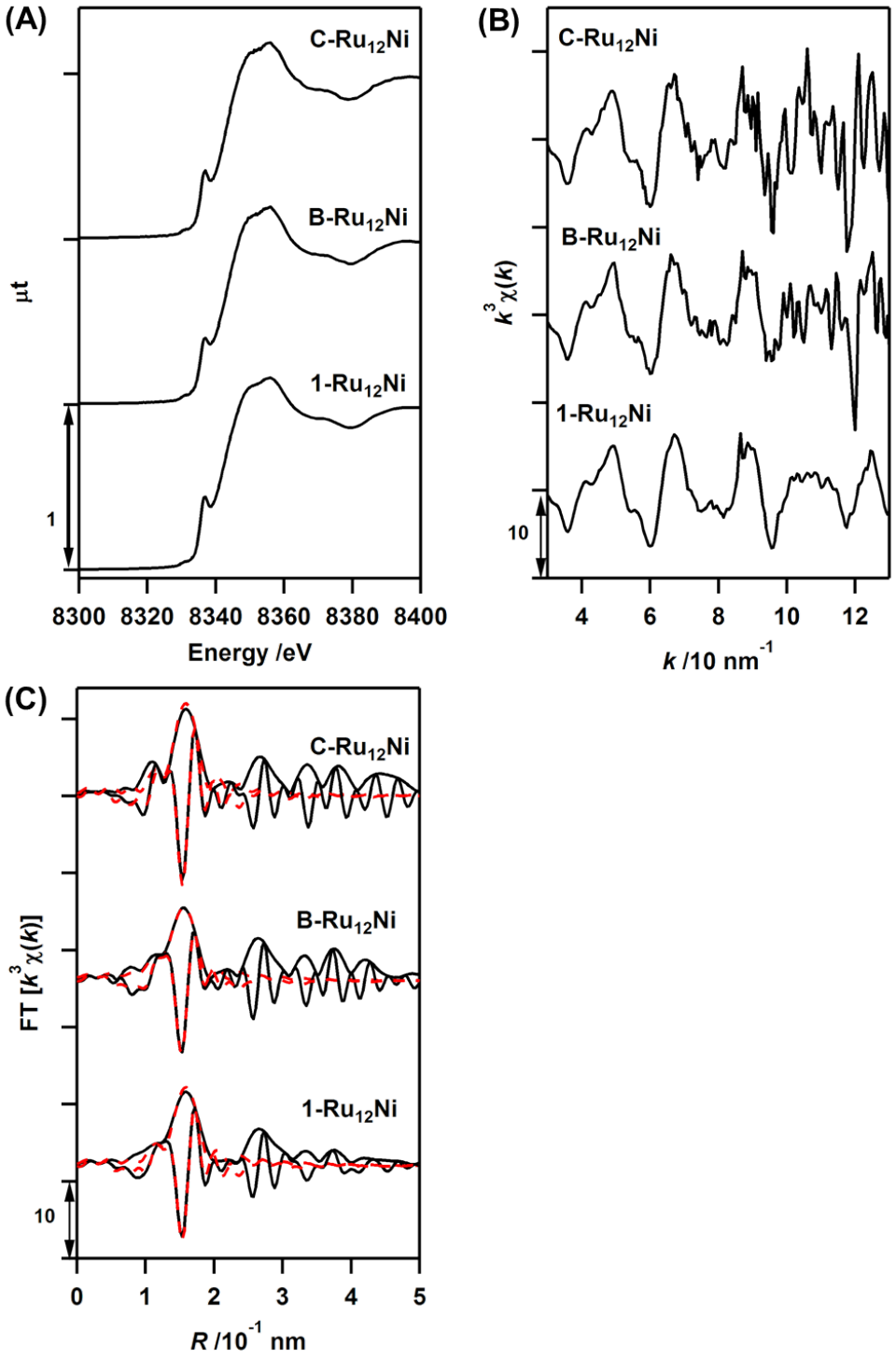

Fig. S6. (A) Normalized Ni K-edge XANES spectra, (B) k^3-weighted Ni K-edge EXAFS oscillations, and (C) their Fourier transforms (k = 30–130 nm^{-1}) for **1-Ru$_{12}$Ni**, **B-Ru$_{12}$Ni**, and **C-Ru$_{12}$Ni**. All of the samples were measured at 20 K. In (C), the black solid lines show the observed data and the red dashed lines show the fitted data.

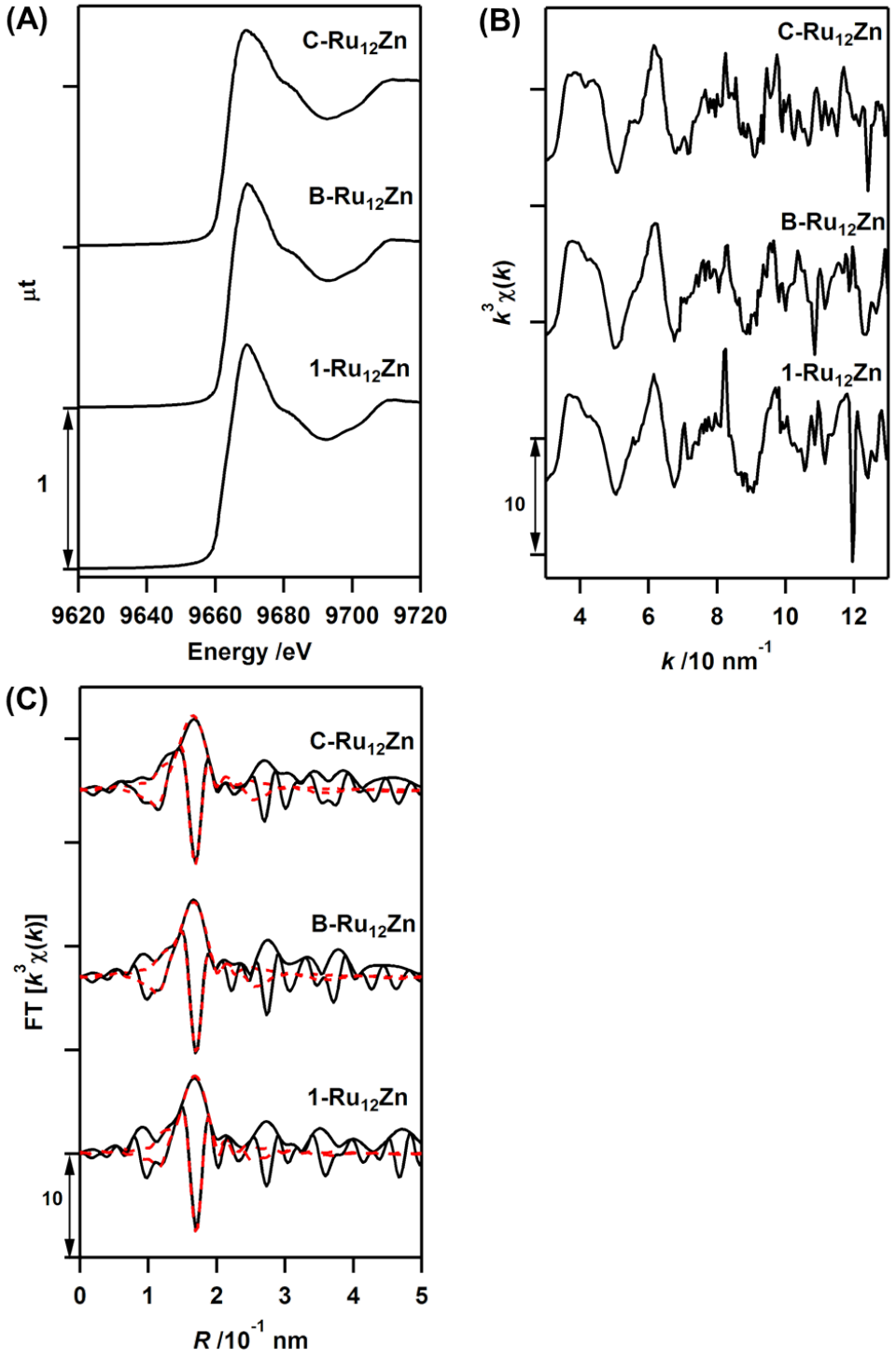

Fig. S7. (A) Normalized Zn K-edge XANES spectra, (B) k^3-weighted Zn K-edge EXAFS oscillations, and (C) their Fourier transforms (k = 30–130 nm^{-1}) for **1-Ru$_{12}$Zn**, **B-Ru$_{12}$Zn**, and **C-Ru$_{12}$Zn**. All of the samples were measured at 20 K. In (C), the black solid lines show the observed data and the red dashed lines show the fitted data.

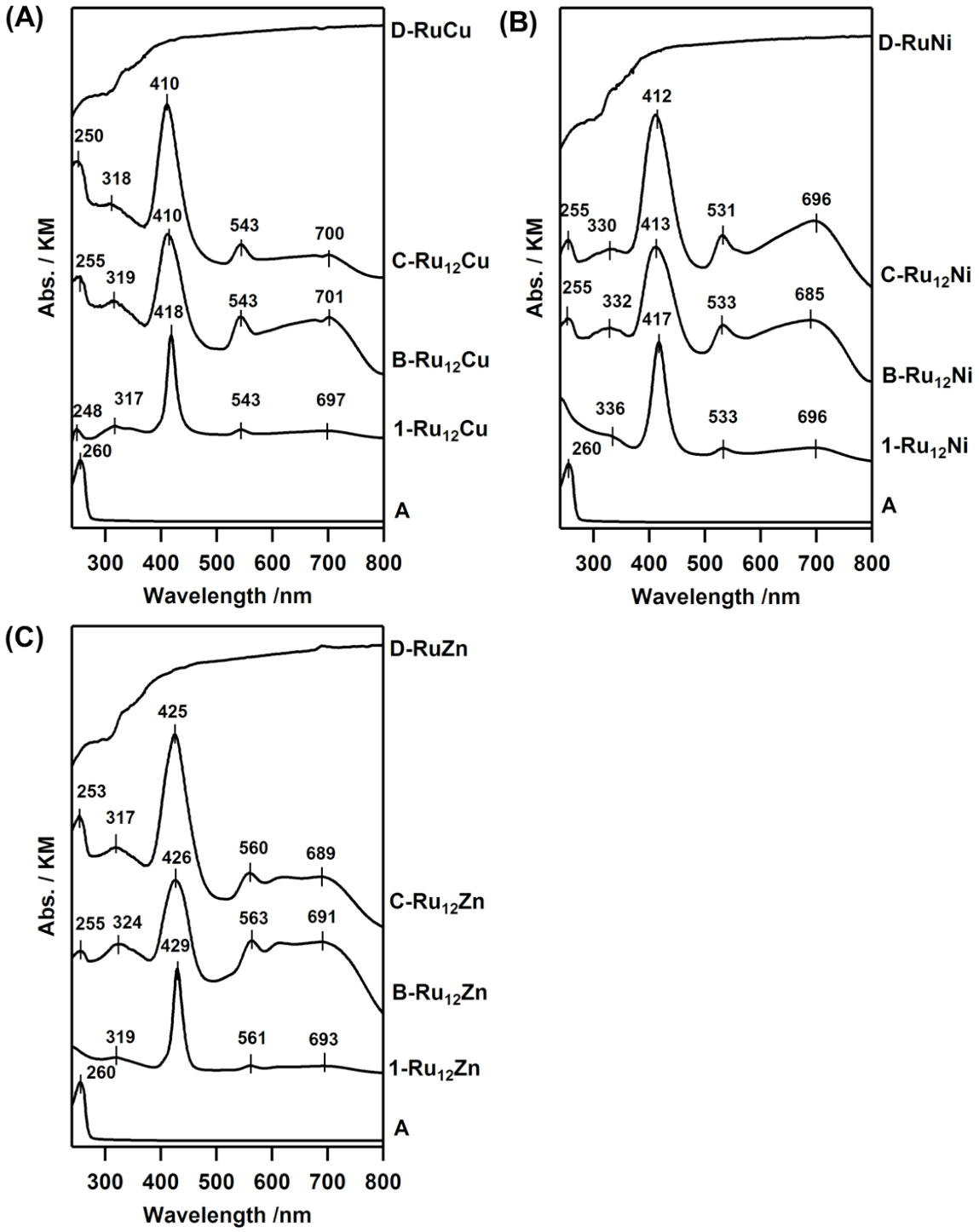

Fig. S8. (A) UV/vis spectrum of **1-Ru_{12}Cu** (in dichloromethane) and DR UV/vis spectra of **A**, **B-Ru_{12}Cu**, **C-Ru_{12}Cu**, and **D-RuCu**. (B) UV/vis spectrum of **1-Ru_{12}Ni** (in dichloromethane) and DR UV/vis spectra of **A**, **B-Ru_{12}Ni**, **C-Ru_{12}Ni**, and **D-RuNi**. (C) UV/vis spectrum of **1-Ru_{12}Zn** (in dichloromethane) and DR UV/vis spectra of **A**, **B-Ru_{12}Zn**, **C-Ru_{12}Zn**, and **D-RuZn**.

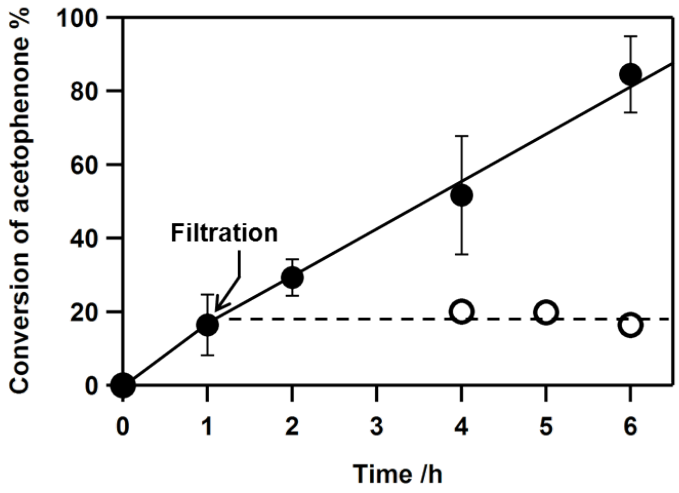

Fig. S9. Conversion of acetophenone for various reaction times on **D-RuCu** (●: Data from individual batch, not time-course measurements), and test of the heterogeneous nature of **D-RuCu** in the hydrogenation of acetophenone (○: Data of continuous reaction in the filtrate after the filtration of the solid catalyst at 20% conversion). Ru = 1.1×10^{-6} mol, Ru/acetophenone/dodecane (internal standard) = 1/500/250 (molar ratio), 0.18 mol L^{-1} of acetophenone in 1,4-dioxane, 363 K, 2.0 MPa of H_2, The amounts of the reactant and products were evaluated by GC and GC-MS with internal standard method.

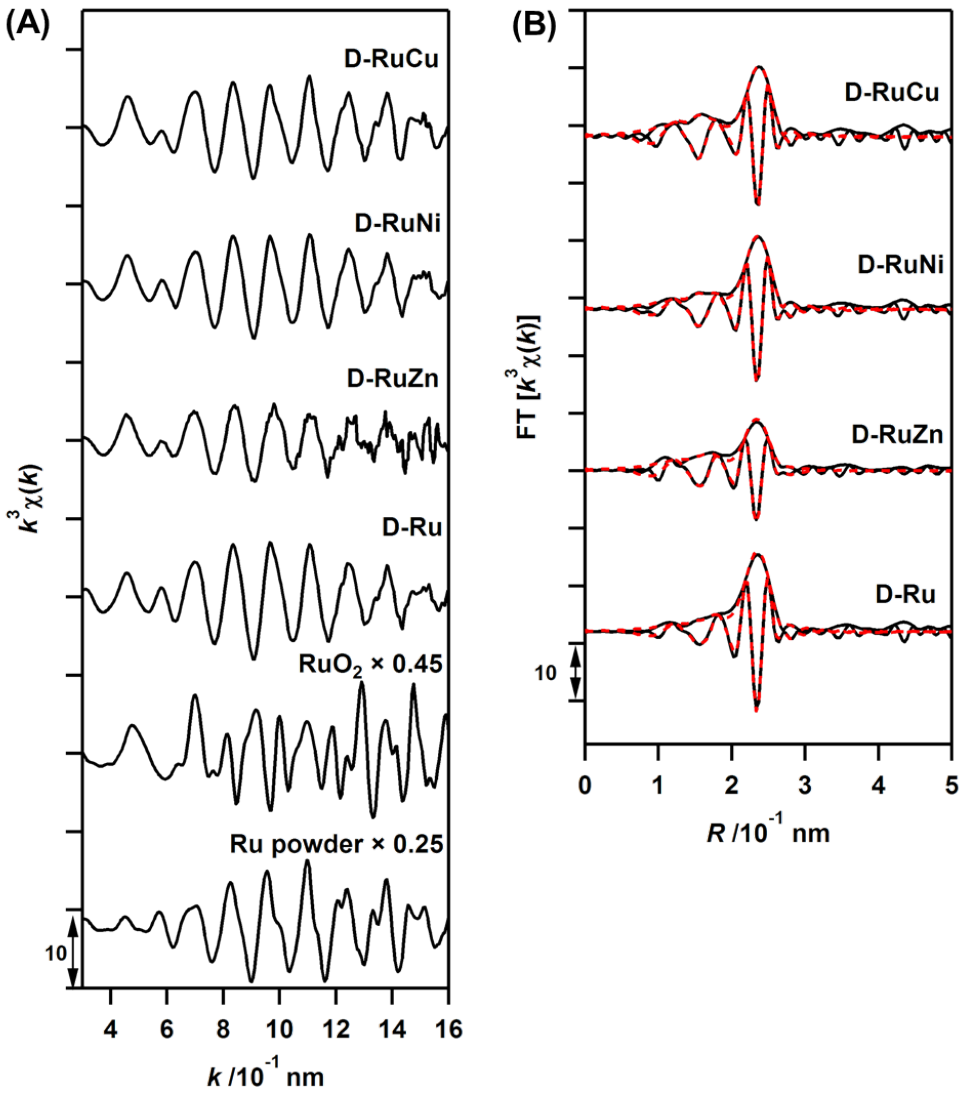

Fig. S10. (A) k^3-Weighted Ru K-edge EXAFS oscillations for **D-RuCu**, **D-RuNi**, **D-RuZn**, **D-Ru**, RuO_2, and Ru powder, and (B) their Fourier transforms (k = 30–160 nm^{-1}) for **D-RuCu**, **D-RuNi**, **D-RuZn**, and **D-Ru**. All of the samples were measured at 20 K. In (B), the black solid lines show the observed data and the red dashed lines show the fitted data.

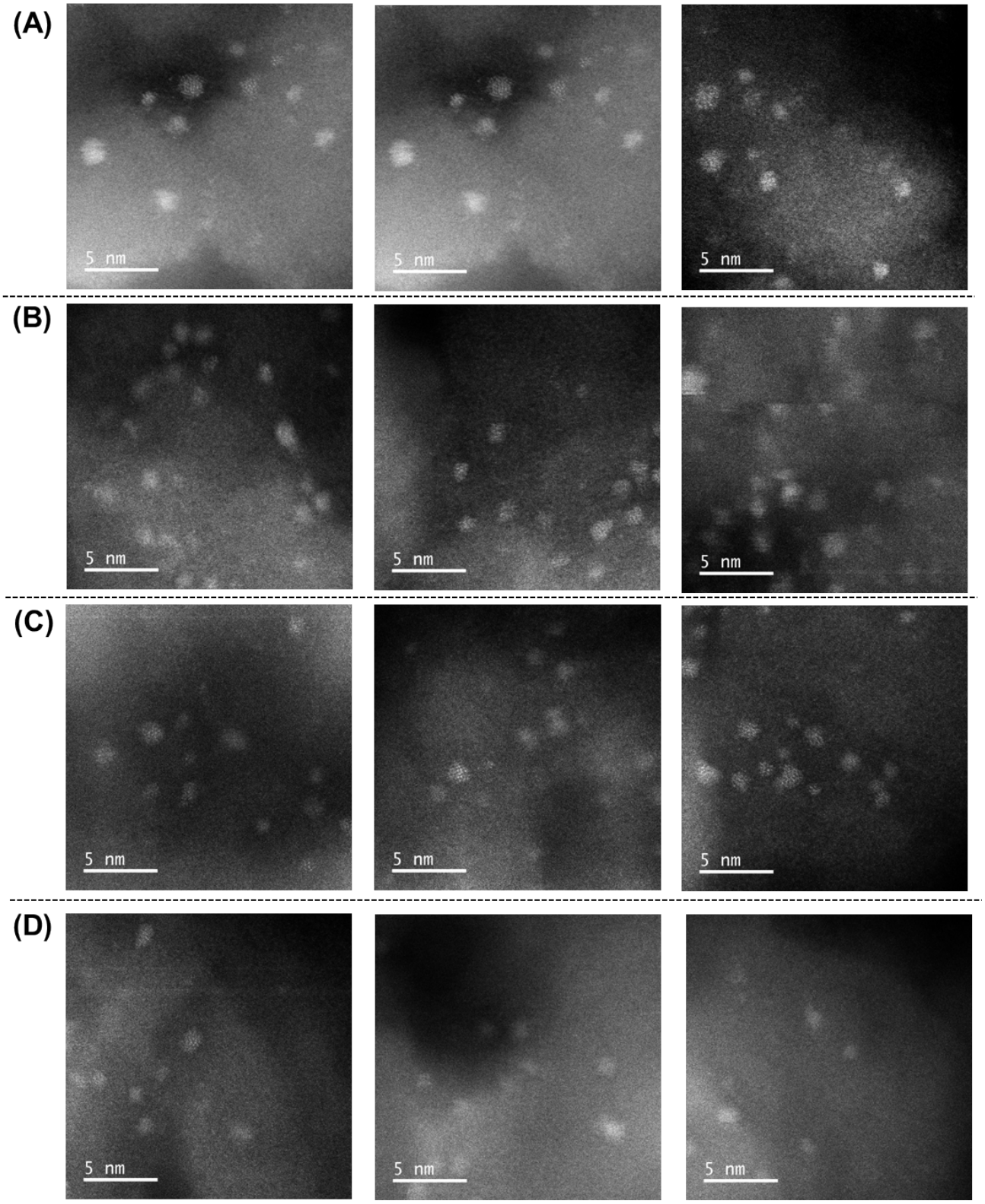

Fig. S11. HAADF-STEM images of (A) **D-RuCu**, (B) **D-RuNi**, (C) **D-RuZn**, and (D) **D-Ru**.

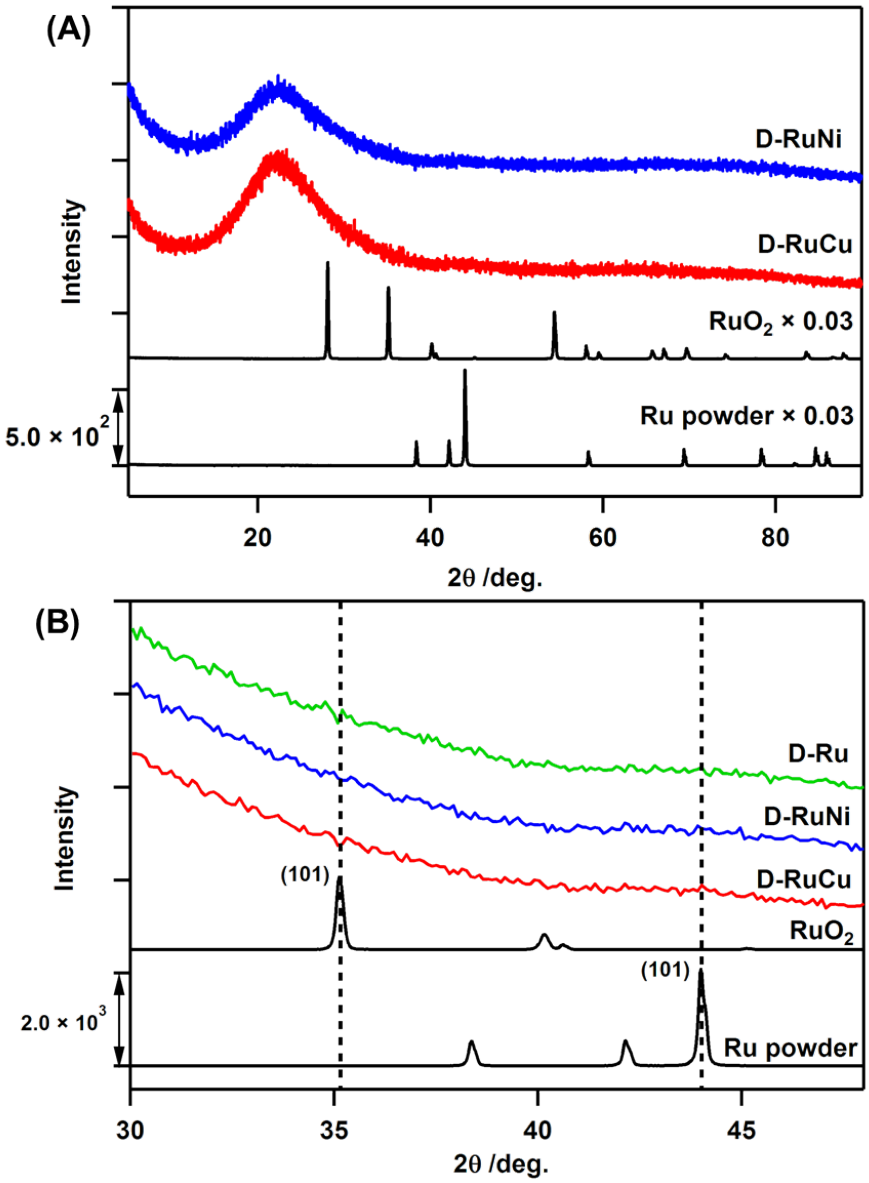

Fig. S12. (A) Wide-angle XRD spectra of Ru powder, RuO_2, **D-RuCu**, and **D-RuNi**. (B) Narrow-angle XRD spectra of Ru powder, RuO_2, **D-RuCu**, **D-RuNi**, and **D-Ru**.

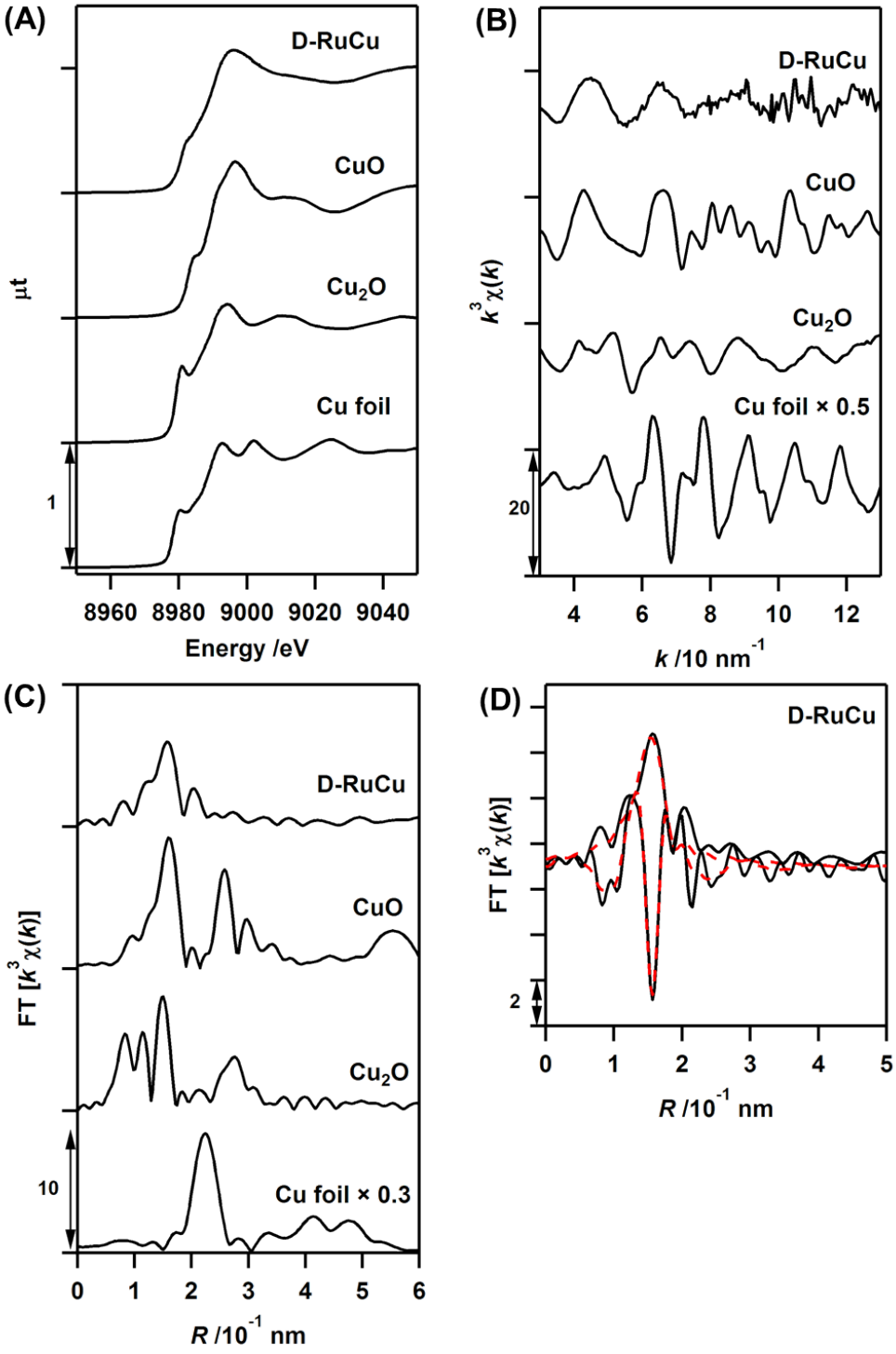

Fig. S13. (A) Normalized Cu K-edge XANES spectra, (B) k^3-weighted Cu K-edge EXAFS oscillations, and (C) their Fourier transforms for **D-RuCu**, CuO, Cu_2O, and Cu foil. All of the samples were measured at 20 K. (D) Curve-fitting data for the k^3-weighted Cu K-edge EXAFS Fourier transform (k = 30–130 nm^{-1}) for **D-RuCu**. In (D), the black solid lines show the observed data and the red dashed lines show the fitted data.

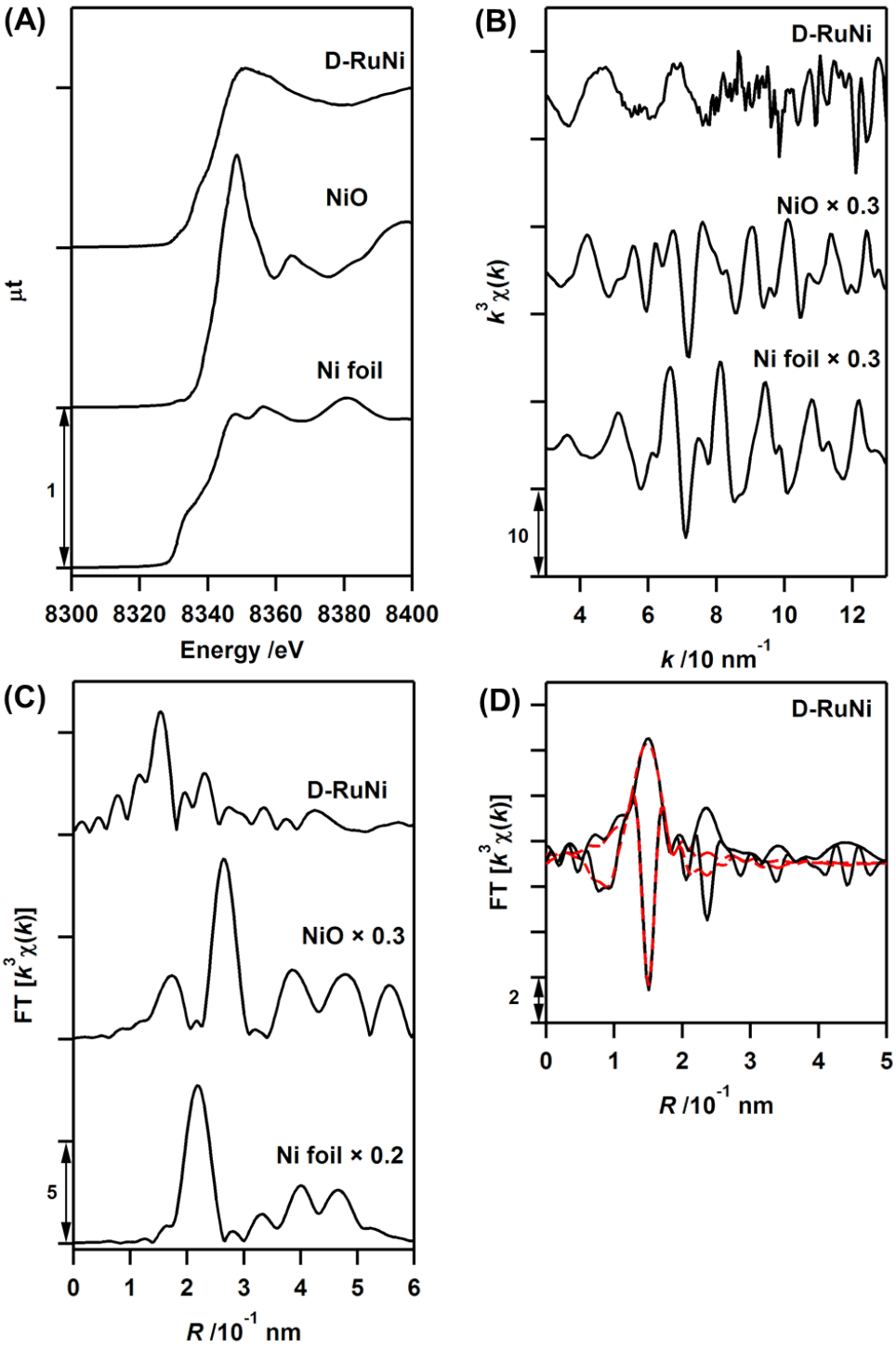

Fig. S14. (A) Normalized Ni K-edge XANES spectra, (B) k^3-weighted Ni K-edge EXAFS oscillations, and (C) their Fourier transforms for **D-RuNi**, NiO, and Ni foil. All of the samples were measured at 20 K. (D) Curve-fitting data for the k^3-weighted Ni K-edge EXAFS Fourier transform (k = 30–120 nm^{-1}) for **D-RuNi**. In (D), the black solid lines show the observed data and the red dashed lines show the fitted data.

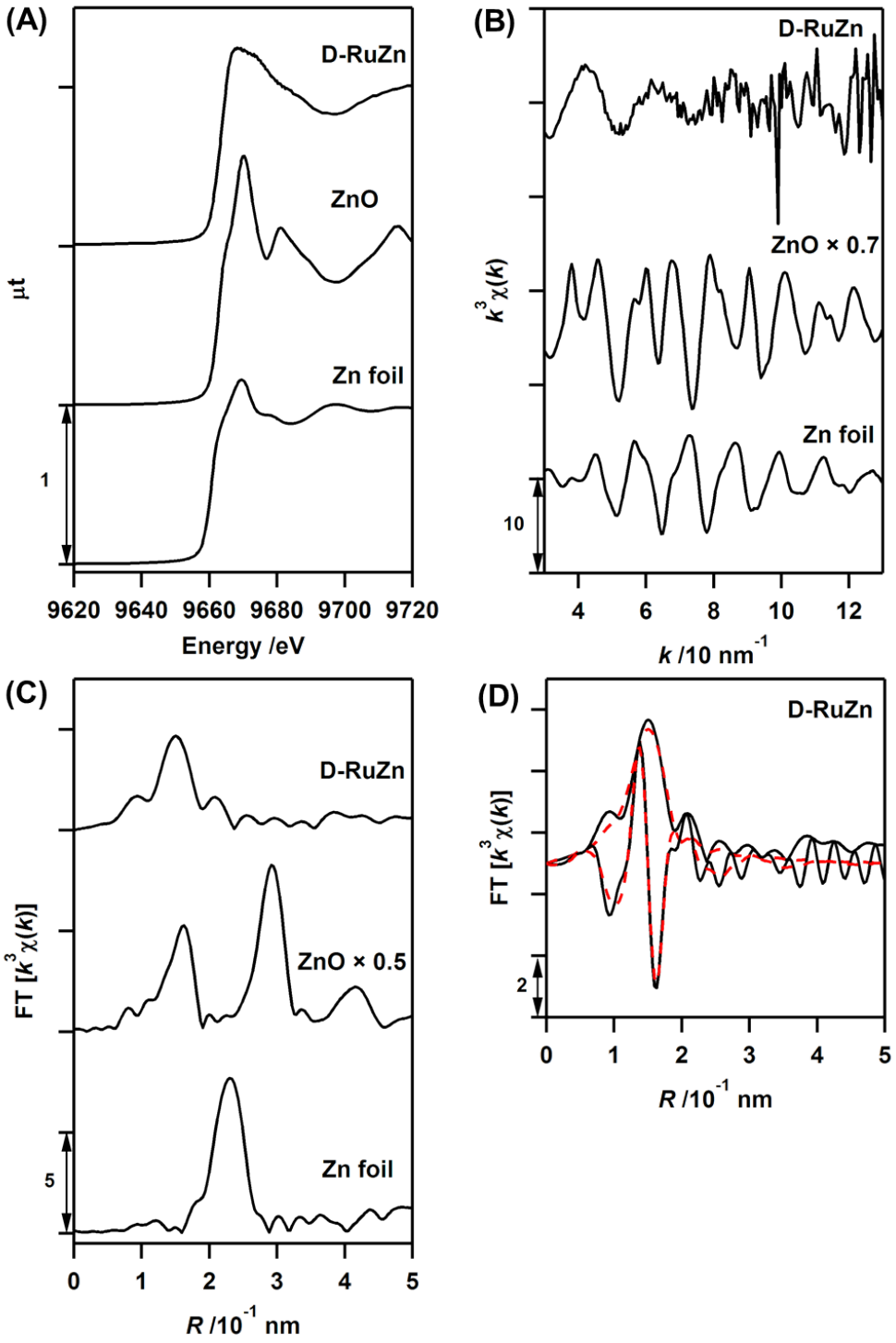

Fig. S15. (A) Normalized Zn K-edge XANES spectra, (B) k^3-weighted Zn K-edge EXAFS oscillations, and (C) their Fourier transforms for **D-RuZn**, ZnO, and Zn foil. All of the samples were measured at 20 K. (D) Curve-fitting data for the k^3-weighted Ni K-edge EXAFS Fourier transform (k = 30–105 nm^{-1}) for **D-RuZn**. In (D), the black solid lines show the observed data and the red dashed lines show the fitted data.

Table S1. Summary of XRF Data

Sample	Ru / wt %	M / wt %
B-Ru_{12}Cu	1.2 ± 0.2	0.06 ± 0.04 (Cu)
B-Ru_{12}Ni	1.2 ± 0.2	0.06 ± 0.04 (Ni)
B-Ru_{12}Zn	1.2 ± 0.2	0.09 ± 0.07 (Zn)
C-Ru_{12}Cu	0.68 ± 0.03	0.04 ± 0.02 (Cu)
C-Ru_{12}Ni	0.70 ± 0.05	0.03 ± 0.02 (Ni)
C-Ru_{12}Zn	0.70 ± 0.03	0.06 ± 0.05 (Zn)
D-RuCu	0.72 ± 0.07	0.04 ± 0.02 (Cu)
D-RuNi	0.73 ± 0.04	0.03 ± 0.02 (Ni)
D-RuZn	0.82 ± 0.05	0.05 ± 0.03 (Zn)

Table S2. Structural Parameters Obtained by Curve-fitting Analysis of Ru K-edge EXAFS Measured at 20 K[a]

Shell	CN	R / nm	ΔE_0	σ^2 / 10^5 nm^2
		1-Ru$_{12}$Cu[b]		
Ru···Ru	1.9 ± 0.6	0.334 ± 0.001	−3 ± 4	3 ± 1
Ru–O (μ-O)	1.0 ± 0.2	0.193 ± 0.006	−2 ± 3	3 ± 2
Ru–O (CH_3COO)	4.0 ± 0.7	0.205 ± 0.004	−2 ± 3	3 ± 2
Ru–N (py)	1.0 ± 0.2	0.209 ± 0.018	−2 ± 3	3 ± 2
Ru···C (CH_3COO, py)	6.0 ± 1.0	0.303 ± 0.002	−2 ± 3	3 ± 2
		B-Ru$_{12}$Cu[c]		
Ru···Ru	1.8 ± 0.6	0.334 ± 0.001	−3 ± 4	2 ± 1
Ru–O (μ-O)	1.1 ± 0.2	0.191 ± 0.005	−3 ± 3	3 ± 2
Ru–O (CH_3COO)	4.3 ± 0.8	0.205 ± 0.002	−3 ± 3	3 ± 2
Ru–N (py)	1.1 ± 0.2	0.203 ± 0.010	−3 ± 3	3 ± 2
Ru···C (CH_3COO, py)	6.4 ± 1.2	0.303 ± 0.002	−3 ± 3	3 ± 2
		C-Ru$_{12}$Cu[d]		
Ru···Ru	1.2 ± 0.6	0.335 ± 0.002	−1 ± 6	3 ± 2
Ru–O (μ-O)	1.1 ± 0.2	0.190 ± 0.006	−3 ± 3	4 ± 1
Ru–O (CH_3COO)	4.3 ± 0.8	0.205 ± 0.009	−3 ± 3	4 ± 1
Ru–N (py)	1.1 ± 0.2	0.206 ± 0.040	−3 ± 3	4 ± 1
Ru···C (CH_3COO, py)	6.5 ± 1.2	0.302 ± 0.002	−3 ± 3	4 ± 1
		1-Ru$_{12}$Ni[e]		
Ru···Ru	2.0 ± 0.7	0.334 ± 0.001	0 ± 4	3 ± 1
Ru–O (μ-O)	1.1 ± 0.2	0.189 ± 0.004	−2 ± 2	3 ± 2
Ru–O (CH_3COO)	4.4 ± 0.7	0.204 ± 0.004	−2 ± 2	3 ± 2
Ru–N (py)	1.1 ± 0.2	0.204 ± 0.020	−2 ± 2	3 ± 2
Ru···C (CH_3COO, py)	6.7 ± 1.1	0.302 ± 0.002	−2 ± 2	3 ± 2
		B-Ru$_{12}$Ni[f]		
Ru···Ru	1.9 ± 0.7	0.334 ± 0.001	−1 ± 4	3 ± 1
Ru–O (μ-O)	1.1 ± 0.2	0.190 ± 0.004	−2 ± 3	3 ± 2
Ru–O (CH_3COO)	4.4 ± 0.7	0.205 ± 0.001	−2 ± 3	3 ± 2
Ru–N (py)	1.1 ± 0.2	0.201 ± 0.007	−2 ± 3	3 ± 2
Ru···C (CH_3COO, py)	6.6 ± 1.1	0.302 ± 0.002	−2 ± 3	3 ± 2
		C-Ru$_{12}$Ni[g]		
Ru···Ru	1.4 ± 0.7	0.334 ± 0.002	−1 ± 5	3 ± 2
Ru–O (μ-O)	1.1 ± 0.2	0.190 ± 0.004	−3 ± 3	3 ± 2
Ru–O (CH_3COO)	4.4 ± 0.8	0.205 ± 0.002	−3 ± 3	3 ± 2
Ru–N (py)	1.1 ± 0.2	0.203 ± 0.011	−3 ± 3	3 ± 2
Ru···C (CH_3COO, py)	6.6 ± 1.2	0.302 ± 0.002	−3 ± 3	3 ± 2
		1-Ru$_{12}$Zn[h]		

Ru···Ru	1.9 ± 0.6	0.334 ± 0.001	−6 ± 4	2 ± 1
Ru–O (μ-O)	0.9 ± 0.2	0.194 ± 0.005	−4 ± 3	2 ± 2
Ru–O (CH_3COO)	3.6 ± 0.8	0.205 ± 0.007	−4 ± 3	2 ± 2
Ru–N (py)	0.9 ± 0.2	0.207 ± 0.028	−4 ± 3	2 ± 2
Ru···C (CH_3COO, py)	5.4 ± 1.2	0.304 ± 0.002	−4 ± 3	2 ± 2
		B-$Ru_{12}Zn$[i]		
Ru···Ru	2.0 ± 0.7	0.332 ± 0.001	−6 ± 4	3 ± 1
Ru–O (μ-O)	1.1 ± 0.2	0.191 ± 0.004	−6 ± 3	2 ± 2
Ru–O (CH_3COO)	4.2 ± 0.7	0.205 ± 0.001	−6 ± 3	2 ± 2
Ru–N (py)	1.1 ± 0.2	0.201 ± 0.007	−6 ± 3	2 ± 2
Ru···C (CH_3COO, py)	6.3 ± 1.0	0.302 ± 0.002	−6 ± 3	2 ± 2
		C-$Ru_{12}Zn$[j]		
Ru···Ru	1.4 ± 0.6	0.335 ± 0.002	−3 ± 5	2 ± 1
Ru–O (μ-O)	1.1 ± 0.2	0.191 ± 0.006	−4 ± 3	4 ± 2
Ru–O (CH_3COO)	4.4 ± 0.8	0.205 ± 0.007	−4 ± 3	4 ± 2
Ru–N (py)	1.1 ± 0.2	0.206 ± 0.031	−4 ± 3	4 ± 2
Ru···C (CH_3COO, py)	6.5 ± 1.2	0.302 ± 0.002	−4 ± 3	4 ± 2
		1-Ru_{12}[k]		
Ru···Ru	1.9 ± 0.6	0.335 ± 0.001	−4 ± 3	3 ± 1
Ru–O (μ-O)	1.0 ± 0.2	0.191 ± 0.005	−4 ± 2	3 ± 2
Ru–O (CH_3COO)	4.2 ± 0.7	0.205 ± 0.004	−4 ± 2	3 ± 2
Ru–N (py)	1.0 ± 0.2	0.205 ± 0.016	−4 ± 2	3 ± 2
Ru···C (CH_3COO, py)	6.3 ± 1.0	0.303 ± 0.002	−4 ± 2	3 ± 2
		B-Ru_{12}[l]		
Ru···Ru	2.0 ± 0.7	0.334 ± 0.001	−5 ± 4	3 ± 1
Ru–O (μ-O)	1.1 ± 0.2	0.191 ± 0.004	−4 ± 3	3 ± 2
Ru–O (CH_3COO)	4.3 ± 0.6	0.206 ± 0.001	−4 ± 3	3 ± 2
Ru–N (py)	1.1 ± 0.2	0.201 ± 0.006	−4 ± 3	3 ± 2
Ru···C (CH_3COO, py)	6.4 ± 0.9	0.303 ± 0.002	−4 ± 3	3 ± 2
		C-Ru_{12}[m]		
Ru···Ru	1.4 ± 0.9	0.334 ± 0.002	−3 ± 7	3 ± 2
Ru–O (μ-O)	1.1 ± 0.2	0.190 ± 0.005	−4 ± 3	3 ± 2
Ru–O (CH_3COO)	4.3 ± 0.7	0.206 ± 0.001	−4 ± 3	3 ± 2
Ru–N (py)	1.1 ± 0.2	0.202 ± 0.008	−4 ± 3	3 ± 2
Ru···C (CH_3COO, py)	6.4 ± 1.1	0.302 ± 0.003	−4 ± 3	3 ± 2
		D-RuCu[n]		
Ru–Ru	3.4 ± 0.3	0.267 ± 0.001	3 ± 1	6 ± 1
Ru–O	1.3 ± 0.6	0.183 ± 0.004	0 ± 4	8 ± 3
Ru–O	3.2 ± 1.2	0.200 ± 0.002	0 ± 4	8 ± 3

		D-RuNi[o]		
Ru–Ru	3.8 ± 0.3	0.266 ± 0.001	2 ± 1	6 ± 1
Ru–O	1.3 ± 0.6	0.183 ± 0.005	0 ± 5	11 ± 4
Ru–O	3.2 ± 1.4	0.202 ± 0.003	0 ± 5	11 ± 4
		D-RuZn[p]		
Ru–Ru	3.6 ± 0.8	0.265 ± 0.001	1 ± 3	8 ± 1
Ru–O	1.4 ± 0.9	0.185 ± 0.005	0 ± 4	9 ± 7
Ru–O	2.9 ± 2.0	0.204 ± 0.004	0 ± 4	9 ± 7
		D-Ru[q]		
Ru–Ru	4.7 ± 0.5	0.266 ± 0.001	1 ± 1	7 ± 1
Ru–O	1.2 ± 1.2	0.186 ± 0.008	0 ± 9	11 ± 10
Ru–O	2.3 ± 2.1	0.206 ± 0.006	0 ± 9	11 ± 10

[a] S_0^2 was fixed to be 1. k = 30–160 nm^{-1}. [b] R = 0.10–0.35 nm, R_f = 2.1%. [c] R = 0.10–0.35 nm, R_f = 2.3%. [d] R = 0.10–0.35 nm, R_f = 3.6%. [e] R = 0.10–0.35 nm, R_f = 2.4%. [f] R = 0.10–0.35 nm, R_f = 2.7%. [g] R = 0.10–0.35 nm, R_f = 3.1%. [h] R = 0.10–0.35 nm, R_f = 2.8%. [i] R = 0.10–0.35 nm, R_f = 2.5%. [j] R = 0.10–0.35 nm, R_f = 3.0%. [k] R = 0.10–0.35 nm, R_f = 1.9%. [l] R = 0.10–0.35 nm, R_f = 2.4%. [m] R = 0.10–0.35 nm, R_f = 4.6%. [n] R = 0.10–0.28 nm, R_f = 0.6%. [o] R = 0.10–0.28 nm, R_f = 0.4%. [p] R = 0.10–0.28 nm, R_f = 2.1%. [q] R = 0.10–0.28 nm, R_f = 0.8%.

Table S3. Structural Parameters Obtained by Curve-fitting Analysis of Cu K-edge EXAFS Measured at 20 K

Shell	CN	R / nm	ΔE_0	σ^2 / 10^5 nm^2
		1-Ru$_{12}$Cu[a]		
Cu–N (porphyrin)	4	0.199 ± 0.001	4 ± 3	2 ± 1
		B-Ru$_{12}$Cu[b]		
Cu–N (porphyrin)	3.5 ± 0.5	0.199 ± 0.001	4 ± 3	3 ± 1
		C-Ru$_{12}$Cu[c]		
Cu–N (porphyrin)	3.7 ± 0.3	0.199 ± 0.001	4 ± 1	3 ± 1
		D-RuCu[d]		
Cu–O	3.4 ± 0.8	0.193 ± 0.002	11 ± 3	7 ± 2

[a] S_0^2 was fitted to be 0.97. k = 30–130 nm^{-1}, R = 0.10–0.20 nm, R_f = 1.7%. [b] S_0^2 was fixed to be 0.97. k = 30–130 nm^{-1}, R = 0.10–0.20 nm, R_f = 1.5%. [c] S_0^2 was fixed to be 0.97. k = 30–130 nm^{-1}, R = 0.10–0.20 nm, R_f = 0.6%. [d] S_0^2 was fixed to be 0.67. k = 30–130 nm^{-1}, R = 0.10–0.19 nm, R_f = 2.5%.

Table S4. Structural Parameters Obtained by Curve-fitting Analysis of Ni K-edge EXAFS Measured at 20 K

Shell	CN	R / nm	ΔE_0	σ^2 / 10^5 nm^2
		1-Ru$_{12}$Ni[a]		
Ni–N (porphyrin)	4	0.194 ± 0.001	6 ± 3	2 ± 1
		B-Ru$_{12}$Ni[b]		
Ni–N (porphyrin)	4.6 ± 0.8	0.193 ± 0.001	4 ± 2	3 ± 1
		C-Ru$_{12}$Ni[c]		
Ni–N (porphyrin)	4.4 ± 0.9	0.194 ± 0.001	5 ± 3	1 ± 1
		D-RuNi[d]		
Ni–O	2.0 ± 0.4	0.188 ± 0.001	9 ± 3	5 ± 2

[a] S_0^2 was fitted to be 0.73. k = 30–130 nm^{-1}, R = 0.10–0.20 nm, R_f = 2.1%. [b] S_0^2 was fixed to be 0.73. k = 30–130 nm^{-1}, R = 0.10–0.20 nm, R_f = 1.1%. [c] S_0^2 was fixed to be 0.73. k = 30–130 nm^{-1}, R = 0.10–0.20 nm, R_f = 2.2%. [d] S_0^2 was fixed to be 0.92. k = 30–120 nm^{-1}, R = 0.10–0.20 nm, R_f = 1.6%.

Table S5. Structural Parameters Obtained by Curve-fitting Analysis of Zn K-edge EXAFS Measured at 20 K

Shell	CN	R / nm	ΔE_0	σ^2 / 10^5 nm^2
		1-Ru$_{12}$Zn[a]		
Zn–N (porphyrin)	4	0.207 ± 0.002	3 ± 3	4 ± 2
		B-Ru$_{12}$Zn[b]		
Zn–N (porphyrin, Py)	5.2 ± 1.1	0.207 ± 0.001	2 ± 2	6 ± 2
		C-RuZn[c]		
Zn–N (porphyrin, Py)	4.9 ± 0.6	0.205 ± 0.001	3 ± 2	6 ± 1
		D-RuZn[d]		
Zn–O	3.2 ± 1.4	0.195 ± 0.004	7 ± 5	10 ± 6

[a] S_0^2 was fitted to be 0.82. k = 30–130 nm^{-1}, R = 0.10–0.20 nm, R_f = 2.4%. [b] S_0^2 was fixed to be 0.82. k = 30–130 nm^{-1}, R = 0.10–0.20 nm, R_f = 1.5%. [c] S_0^2 was fixed to be 0.82. k = 30–130 nm^{-1}, R = 0.10–0.20 nm, R_f = 1.4%. [d] S_0^2 was fixed to be 0.92. k = 30–105 nm^{-1}, R = 0.10–0.20 nm, R_f = 2.0%.

Table S6. Curve-fitting Analysis of Ru $3p_{3/2}$ XPS Spectra

Sample	Binding energy / eV[a]
D-RuCu	462.2
D-RuNi	461.5
D-Ru	461.3
Ru powder	461.1

[a] Each value of binding energy was calibrated using the Si 2p peak.

References

1. J. A. Baumann, D. J. Salmon, S. T. Wilson, T. J. Meyer, W. E. Hatfield, *Inorg. Chem.* 1978, **17**, 3342.

2. N. M. Barbosa Neto, L. De Boni, C. R. Mendonça, L. Misoguti, S. L. Queiroz, L. R. Dinelli, A. A. Batista, S. C. Zilio, *J. Phys. Chem. B* 2005, **109**, 17340.

3. F. J. Pavinatto, A. F. Gameiro Jr., A. A. Hidalgo, L. R. Dinelli, L. L. Romualdo, A. A. Batista, N. M. Barbosa Neto, M. Ferreira, O. N. Oliveira Jr., *Appl. Surf. Sci.* 2008, **254**, 5946.

4. L. R. Dinelli, G. Von Poelhsitz, E. E. Castellano, J. Ellena, S. E. Galembeck, A. A. Batista, *Inorg. Chem.* 2009, **48**, 4692.

5. O. N. Suvorova, G. A. Domrachev, E. A. Shchupak, G. S. Kudryavtseva, A. I. Kirillov, A. A. Zaitsev, *Russ. Chem. Bull., Int. Ed.* 2009, **58**, 2233.

6. S. Dovidauskas, K. Araki, H. E. Toma, *J. Porphyrin. Phthalocyanin.* 2000, **4**, 727.

7. W. Zhang, L. Xing, H. Wang, X. Liu, Y. Feng, C. Gao, *Langmuir* 2015, **31**, 4330.

8. S. Muratsugu, M. H. Lim, T. Itoh, W. Thumrongpatanaraks, M. Kondo, S. Masaoka, T. S. A. Hor, M. Tada, *Dalton Trans.* 2013, **42**, 12611.

9. (a) S. Muratsugu, M. Tada, *Acc. Chem. Res.* 2013, **46**, 300. (b) S. Muratsugu, Z. Weng, M. Tada, *ACS Catal.* 2013, **3**, 2020.

10. (a) B. Ravel, M. Newville, *J. Synchrotron Rad*. 2005, **12**, 537. (b) M. Newville, B. Ravel, D. Haskel, J. J. Rehr, E. A. Stern, Y. Yacoby, *Physica B* 1995, **208-209**, 154.

11. J. A. Bearden, A. F. Burr, *Rev. Mod. Phys.* 1967, **39**, 125.

12. (a) M. Newville, *J. Synchrotron Rad*. 2001, **8**, 322. (b) M. Newville, P. Līviņŝ, Y. Yacoby, J. J. Rehr, E. A. Stern, *Phys. Rev. B* 1993, **47**, 14126.

13. A. L. Ankudinov, B. Ravel, J. J. Rehr, S. D. Conradson, *Phys. Rev. B* 1998, **58**, 7565.

14. J. C. Goeltz, E. E. Benson, C. P. Kubiak, *J. Phys. Chem. B* 2010, **114***,* 14729.

15. H.-S. He, *Acta Crystallogr. Sect. E: Struct. Rep. Online* 2007, **63**, m976.

16. D. L. Cullen, E. F. Meyer Jr., *J. Am. Chem. Soc.* 1974, **96**, 2095.

17. M. N. Alberti, S. Nowakowska, M. D. Tzirakis, J. Nowakowski, P. Fesser, W. B. Schweizer, A. Shchyrba, C. Thilgen, T. A. Jung, F. Diederich, *Eur. J. Org. Chem.* 2014, **26**, 5705.